Neogene subtropical front development in the Tasmania Gateway: implications for ice volume

Universiteit Utrecht
Faculty of Geosciences
Marine palynology & paleoecanography
Contact: p.k.bijl@uu.nl

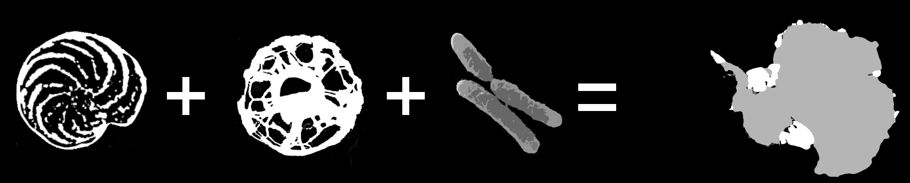

Suning Hou, Ryan Paul, Mei Nelissen, Lennert B. Stap, Frida Hoem, Martin Ziegler, Appy Sluijs, Peter K. Bijl
Utrecht University, Department of Earth Sciences, Utrecht, the Netherlands

Introduction:

The long-term Neogene global cooling is usually thought characterized by Antarctic ice volume increase[1,2,3], pCO_2 decline[4,5,6]. Oceanographic changes also occurred, specially the strengthening of the latitudinal temperature gradient[7] and the development of Antarctic Circumpolar Current (ACC) and associated oceanic fronts[8,9,10], in particular the subtropical front (STF).
Yet, the history of the ACC and associated fronts is poorly constrained and carbonate clumped isotopes have provided new estimates on ice volume reconstruction. Hereby, we use a suite of tools to reconstruct the paleoenvironment at ODP Site 1168 (Fig. 1). This includes a novel dinocyst model[11,12] (Fig. 2) indicating the dynamics of the STF, and clumped isotope of benthic foraminifera reflecting bottom water temperature (BWT). Subsequently we use these to estimate the global ice volume. Our study demonstrates the complex interactions between Antarctic ice sheet and Southern Ocean surface and deep oceanographic changes

Methods:

1. Dinocyst assembalges indicate oceanographic change
2. Biomarker-based proxies reconstruct sea (sub)surface temperature (SST)
3. Clumped and stable isotopes of benthic foraminifera indicate BWT and ice volume.

Site description: ODP Site 1168

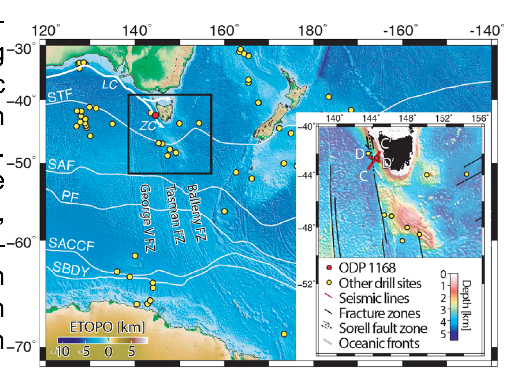

Figure 1. (a) Pesent-day map of the Australian sector of the southern ocean showing ODP Site 1168, other drilling sites, oceanic fronts and currents. (b) Seismic section crossing Site 1168 with lithological units. STF is the subtropical front, PF is the polar front, SAF is the subantarctic front, SACCF is the Southern Antarctic Circumpolar Current front and SBDY is the southern boundary) and southern Australian ocean currents (white arrow; LC is the Leeuwin Current and ZC is the Zeehan Current)[7].

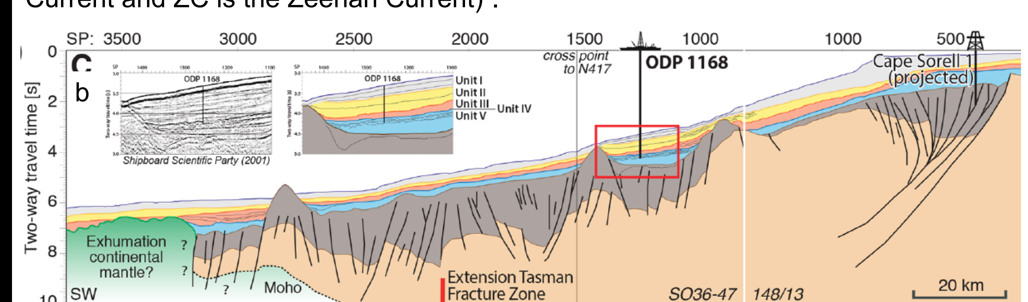

Dinocyst cluster model of the Southern Ocean

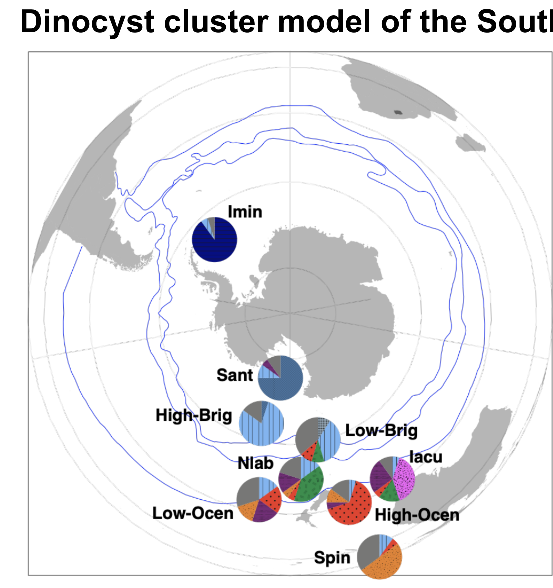

Figure 2. Distribution of different dinocyst assemblage clusters and ACC frontal systems in the modern Southern Ocean[12]. blue colors represen taxa specific for upwelling- and seaice-proximal conditions, green taxa occur southeof the STF, and red/purple species north of the STF.

Dinoflagellate cyst assemblage of Site 1168

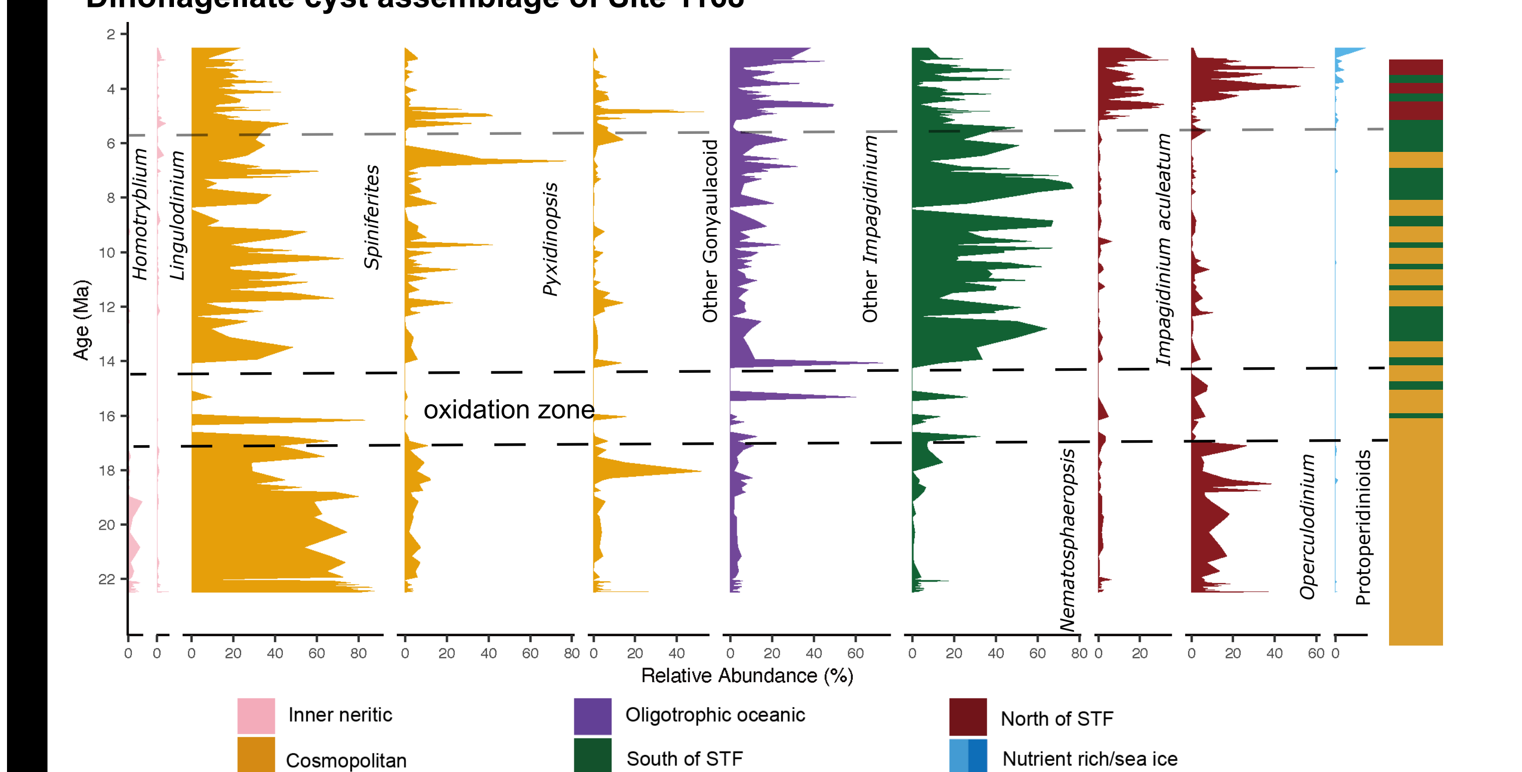

Figure 3. Relative abundance (%) of selected dinocyst taxa and/or groups. Dinocyst taxa have been assigned to an ecological group (see legend). Dinocyst assemblage has been identified as clusters.

Development of the STF based on dinocyst assemblages

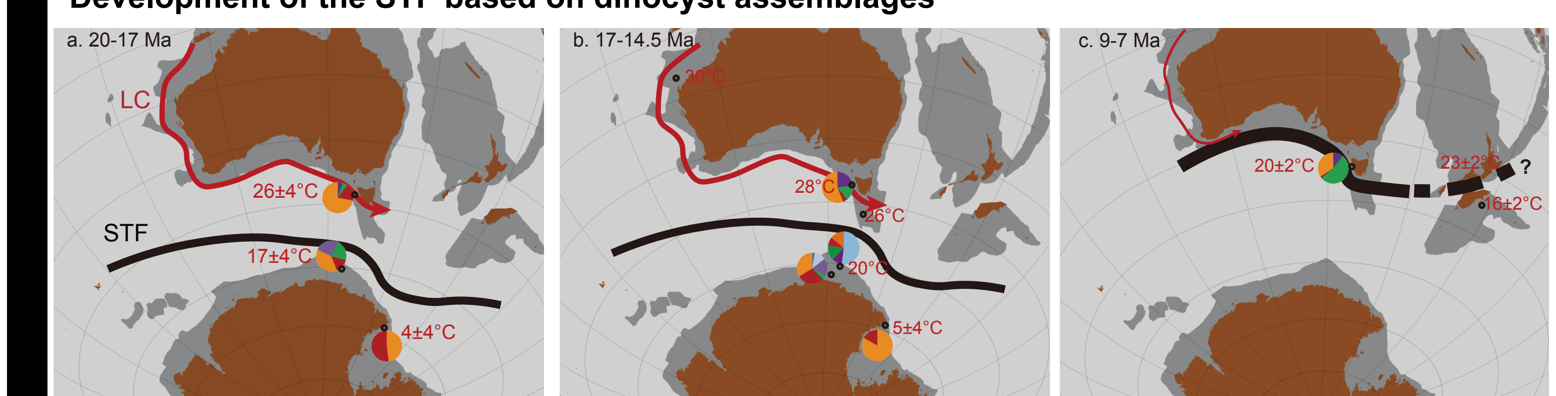

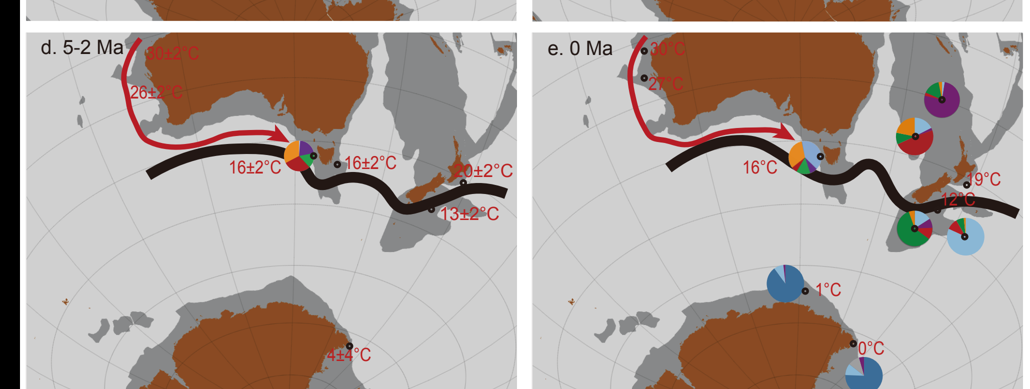

Figure 4. Dinocyst biogeographic patterns in the Neogene Tasmanian sector (a) early Miocene 20-17 Ma; (b) MCO 17-14.5 Ma; (c) late Miocene 9-7 Ma; (d) Pliocene 5-2 Ma (e), Modern 0 Ma, from ODP Site 1168 and other studies (e.g. Site U1356, Site 269, AND-2A)[9,11,13,14,15]. From this we reconstructed the paleoposition of the Leeuwin Current and STF. Thickness of the lines indicates current strength. Abbreviations follow Fig. 1, dinocyst colour code follows Fig. 2.

Results:

1. Dinocyst assemblages (Fig. 3) after the Miocene Climatic Optimum (MCO) imply a northward migration of the STF (Fig. 4), concomitant to progressive ~10°C cooling of the SH mid-latitudes (Fig. 6a). Orbital-timescale variability reflects glacial-interglacial cyclicity in the latitudinal position of the STF (Fig. 3).

2. BWT first decreased (8–3°C) from MCO to 9 Ma, then increased back to the MCO level at 8 Ma, decreasing to 4°C at the end of the Miocene. Seawater $\delta^{18}O$ was relatively constant around present-day value 17–9 Ma, with perhaps some global ice volume increase between 9 and 8 Ma (Fig. 6b, c).

BWT and ice volume reconstruction based on clumped isotopes

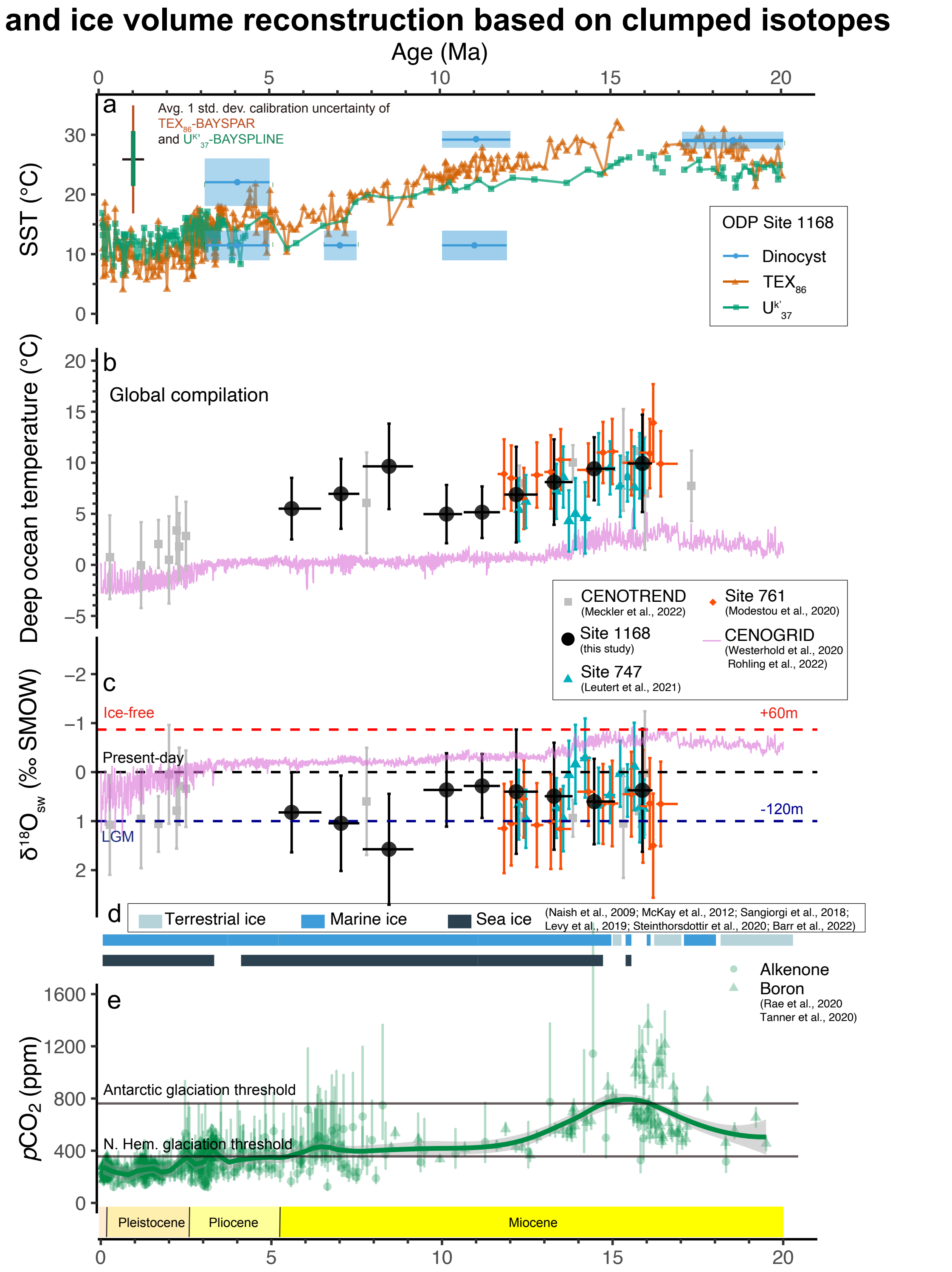

Figure 6. (a). Sea (sub)surface temperature of Site 1168 based on TEX_{86}, U^{K}_{37}[14] and dinocysts. Solid lines indicate loess fit through TEX_{86} and U^{K}_{37}. Blocks indicate the preferential temperature range of modern dinocyst clusters (Fig. 2). (b). Deep-sea temperaure (symbols with error bars) based on clumped isotopes[3,17,19], with the modeled decovolution of $\delta^{18}O$[20] (c). Calculated $\delta^{18}O$ of sea water compared with ice-free, present-day and Last glacial Maximum (LGM) values (dashed lines). Vertical error bar: 95% confidence interval, horizontal bar: time bins. (d) Qualitative geological record of Antarctic land- and sea ice extent (e). pCO_2 compilation from alkenones and boron isotopes[3].

Integration:

How can we reconcile declining benthic d18O, deep-ocean cooling, landice advance towards the ocean, Southern Ocean surface cooling and northwards migration of the subtropical front with an almost stable Antarctic ice volume?

Ice sheet geometry. During MCO, the AA ioce sheet was retreated inland with almost no marine terminations. The regional ocean warmth induced strong precipitation towards the ice sheet, that grew tall with strong surface melt at lower altitude. During the MMCT, the AA ice sheet expanded seawards in area, thereby setting off many local ice-ocean feedbacks that cooled the Southern Ocean and the region of deep-water formation. It also induced snow starvation of the hinterland of the ice sheet, where sublimation continued to lower the altitude of the ice sheet. This kept ice volume constant in spite of areal expansion. Strong intervention in the IMAUICE sheet model was needed in order to simulate such a scenario, but with strong intervention in precipitation and ice-ocean interactions areal extent could come without strong volume change. These simulations are to be followed up with more realistic boundary conditions.

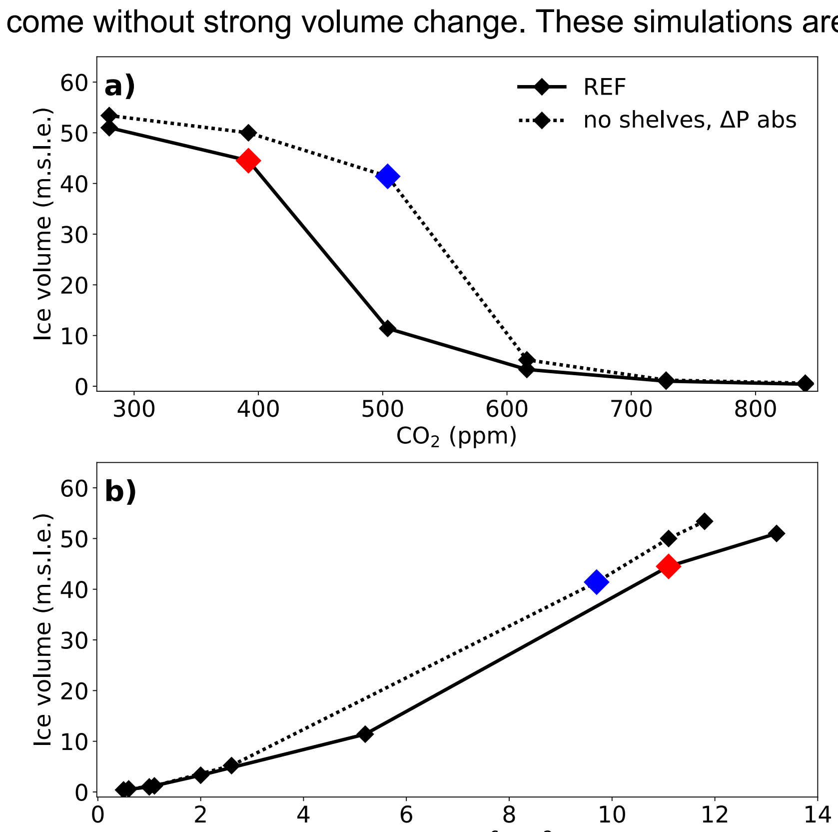

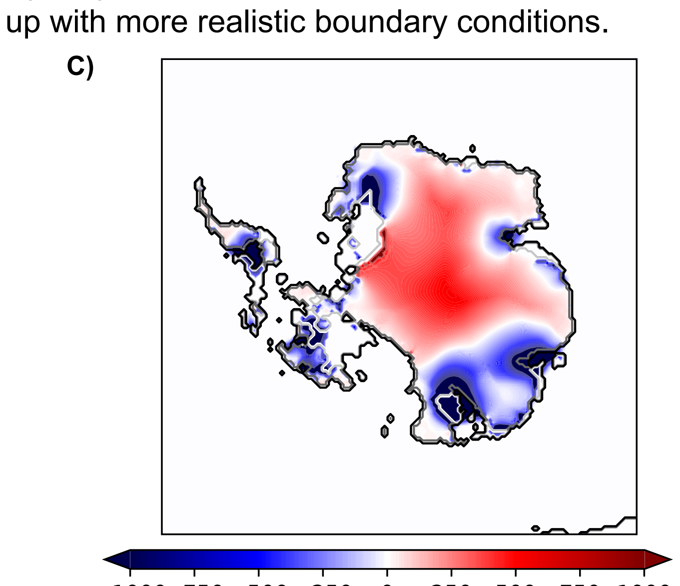

(a) Simulated equilibrated Antarctic ice volumes at different CO2 levels, and (b) the relation between ice volume and ice area, yielded by a 3D thermodynamical ice sheet/shelf model. Results are obtained using the standard climate forcing (solid) and applying a fixed precipitation increase and extreme sub-shelf melt rates (dashed). (c) Equilibrated ice thickness difference between the reference simulation at 392 ppm and the simulation with anomalous forcing at 504ppm. This transition (from the blue to the red symbols) exemplifies our hypothesized Antarctic ice sheet change at the MMCT.

Conclusions:

1. The STF started to strengthen after the MCO then moved northward towards Australia and reached its northmost position around 7 Ma (Fig.4).

2. The post-MCO northward migration of the STF coincided with regional sea (sub)surface cooling which decreased the latitudinal SST gradient between the AA coast and the STF. This phenomenon questions whether climate cooling, and polar amplification of that, really did trigger polar cryosphere expansion, particularly now that evidence from clumped isotopes suggest stable ice volume (Fig. 6).

3. Our data taken together suggests an opposite[21] ice dynamic pattern may exist: Land-based Antarctic ice volume was already close to the modern size despite the warm ocean in the MCO. Subsequently, it expanded on its surface towards the ocean but reduced in height, led to the northward migration of the STF and cooling BWT meanwhile maintaining a relatively stable volume.

Acknowlegements: We thank the International Ocean Discovery Program for samples. This research is supported by the European Research Council starting grant OceaNice to Peter Bijl. We thank Mariska Hoorweg, Klaas Nierop, Desmond Eefting, Natasja Welters, Giovanni Dammers, Arnold van Dijk for their technical support in the lab.

Reference: 1. Lewis et al., 2007
2. Lear et al., 2015
3. Leutert et al., 2021
4. Super et al., 2018
5. Tanner et al., 2020
6. Rae et al., 2021
7. Hou et al., in review
8. Scher et al., 2014
9. Hoem et al., 2021
10. Evangelinos et al., 2021
11. Prebble et al., 2013
12. Thöle et al., 2022
13. Warny et al., 2009
14. Bijl et al., 2018
15. Sangiorgi et al., 2018
16. Westerhold et al., 2020
17. Modestou et al., 2020
18. Christensen et al., 2019
19. Meckler et al., 2022
20. Rohling et al., 2023
21. Bradshaw et al., 2021